Pure Appl. Geophys. 176 (2019), 4555–4573

https://doi.org/10.1007/s00024-019-02281-6

Pure and Applied Geophysics

The Second-Order Derivative of GPS Carrier Phase as a Promising Means for Ionospheric Scintillation Research

Vladislav V. Demyanov,[1,2] Yury V. Yasyukevich,[1,3] Shuanggen Jin,[4] and Maria A. Sergeeva[5,6]

Abstract—The carrier phase observable is the most preferable means for observation of ionospheric scintillation events. As the ionospheric scintillations show different features at different GNSS frequencies the single-frequency data should be used for complex analysis and data interpretation. The second-order derivative of the GPS signal carrier phase is suggested as a promising means to detect small-scale ionospheric disturbances. The high-rate L1 phase data with no additional processing are used for this purpose. Modeling and experimental results proved the hypothesis. It was revealed the strict dependence of sensitivity of the second-order derivative parameter on GPS receiver hardware features and carrier phase sampling rate.

Key words: GPS, ionosphere, scintillation, scintillation indices.

1. Introduction

Rapid temporal fluctuations of the radio signal phase and amplitude (ionospheric scintillations) are introduced by the local features of propagation medium such as random changes of the refraction index. Ionospheric scintillations degrade the performance of radio systems, for instance space-based radars, GNSS applications, communication systems, etc. The problem of the ionospheric scintillations impact on the space-based telecommunication and navigation system performance has been studied for decades (Kintner et al. 2001; Ledvina et al. 2002; Herbster 2007; Afraimovich et al. 2003, 2009, 2013; Tiwari and Strangeways 2015; Juan et al. 2018b). Scintillation activity increases during the periods of high solar activity. In general, scintillations are most pronounced in the equatorial (e.g. provoked by plasma bubbles) and auroral regions (connected mostly to solar and geomagnetic events). At mid-latitudes they can occur during the periods of intense geomagnetic storms (Kintner et al. 2001; Ledvina et al. 2002; Afraimovich and Perevalova 2006; Afraimovich et al. 2009, 2013; Juan et al. 2018b). Other physical phenomena also can cause ionospheric irregularities that provoke scintillations. It is well known that tsunami and powerful earthquakes are usually followed by a combination of atmospheric and ionospheric waves (Afraimovich et al. 2013; Tsugawa et al. 2011; Matsumura et al. 2011; Jin et al. 2017).

There are two types of scintillation effects on radio signal propagating in the ionosphere: rapid fluctuations of signal phase and signal intensity (or carrier-to-noise ratio C/N_0). Correspondent scintillation indices and ionospheric parameters serve for diagnostics of the radio propagation medium to detect the small-scale ionospheric disturbances which provoke these effects. The most "popular" ionospheric parameter derived from GPS data is total electron content (TEC). TEC is reconstructed from dual-frequency GPS phase or code measurements (Jorgenson 1978). Typical ionospheric scintillation indices derived from TEC data are rate of TEC index (ROTI) and its derivative (DROTI) (Pi et al. 1997;

[1] Institute of Solar Terrestrial Physics, Siberian Branch Russian Academy of Sciences, Irkutsk, Russia. E-mail: vv.emyanov@gmail.com
[2] Irkutsk State Transport University, Irkutsk, Russia.
[3] Irkutsk State University, Irkutsk, Russia.
[4] Shanghai Astronomical Observatory, Chinese Academy of Sciences, Shanghai 200030, China.
[5] SCiESMEX, LANCE, Instituto de Geofisica, Unidad Michoacan, Universidad Nacional Autonoma de Mexico, Antigua carretera a Patzcuaro 8701, C.P. 58089 Morelia, Michoacan, Mexico.
[6] CONACYT, Instituto de Geofisica, Unidad Michoacan, Universidad Nacional Autonoma de Mexico, Antigua carretera a Patzcuaro 8701, C.P. 58089 Morelia, Michoacan, Mexico.

Bhattacharrya 2000). Recently, several improved ROTI versions were developed, such as along arc TEC rate (AATR) (Juan et al. 2018a), disturbance ionosphere index (DIX) (Jakowski et al. 2012) and disturbance ionosphere index spatial gradient (DIXSG) (Wilken et al. 2018). There is a new effective scintillation index sDPR (Ghoddousi-Fard et al. 2013; Priyadarshi et al. 2018; Prikryl et al. 2016), that is close to ROTI. It is a good proxy for the weak and moderate scintillation detection and well correlates to the "standard" $\sigma\varphi$ index. The authors (Gulyaeva and Stanislawska 2008; Voeykov et al. 2018) are also suggested the indices to estimate the ionosphere disturbance level.

S4 and the mentioned $\sigma\varphi$ are other widely used scintillation indices. They are the standard deviations of amplitude and phase, respectively (Briggs and Parkin 1963; Yeh and Liu 1982). S4 and $\sigma\varphi$ are calculated based on GPS data and provide scintillation events monitoring with high reliability (Van Dierendonck et al. 1993). As the small-scale ionospheric turbulences have very low intensity, it is very difficult to detect them with TEC observations and TEC-based indices. Reliability of *S4* and $\sigma\varphi$ indices as indicators of the small-scale ionospheric disturbances depends on both the indices computation features and the current ionosphere structure, so sometimes it is not so easy to interpret the results derived from *S4* and $\sigma\varphi$ indices. Thus, it is important to search for new indicators of the weak small-scale structures in the ionosphere. One of the suggested approaches is to use high-rate sampling GPS data (50 Hz or higher) to improve the ionospheric indices sensitivity and reliability for the future ionospheric study. We suggest new scintillation indicator based on high sampling rate GPS (GNSS) data.

In the present work, the second order GPS phase derivative is suggested as a new promising scintillation indicator obtained from GPS data of high sampling rate. The carrier phase observable is the most promising for scintillation research. The carrier phase derivative was introduced as a new parameter in GPS occultation technology (Pavelyev et al. 2010). However, the case of the Earth-Space link is rather different from the case of the occultation links at the standpoint of radio propagation and the impact of Doppler effect. Besides, the ionospheric scintillations show different behavior at different GNSS frequencies. Therefore the data of different frequencies are better analyzed separately to obtain the most exhaustive results in scintillation research. Furthermore, low-frequency trends should be removed from the carrier phase data (Van Dierendonck et al. 1993) before the scintillation indices computation. This data preparation usually involves some additional procedures like carrier phase detrending and cycle-sleep fixing (Van Dierendonck et al. 1993; Cai 2013). In contrast, in the case of high rate carrier phase data, the second-order derivative of the carrier phase can provide an easy way to remove all the low-frequency trends including slow refractive variations, multi-path slow variations, signal encryption effects and other low frequency stochastic biases. On the other hand, the second order derivative of the carrier phase contents high-frequency components including stochastic fluctuations caused by ionospheric phase scintillations.

The aim of this work is to test the hypothesis stated above taking in account the following issues. First, the signal carrier phase scintillations can be caused by not only the ionospheric irregularities but also by a satellite oscillator anomalies and troposphere. Second, the parameter sensitivity crucially depends on the GPS receiver hardware and the carrier phase data sampling rate. In the present study these two issues are discussed and the hypothesis is tested by means of modeling and experimental verification.

2. *Phase Noise Components Evaluation*

As mentioned above, the phase derivative value is calculated at single frequency in contrast to TEC and TEC-based indices. This means that there is no cross-compensation of frequency-independent ranging errors such as troposphere and satellite clock errors. Therefore, the first question to be answered is "How significant are these errors in comparison to the ionospheric phase scintillations?"

The instantaneous phase range value $\left(\Phi_i^k(t) = \varphi_i^k(t)\frac{\lambda}{2\pi}\right)$ for the k-th satellite vehicle (SV) at the ith time point can be expressed as follows (Kaplan 1996):

$$\Phi_i^k(t) = \rho_i^k - I_i^k + T_i^k + \delta m_i^k + c\left(dt_i(t) - dt^k\left(t-\tau_i^k\right)\right) + c\left(\delta_i(t) + \delta^k\left(t-\tau_i^k\right)\right) + \lambda N_i^k + \varepsilon_i^k \quad (1)$$

where ρ_i^k is the phase range corresponding to "SV-receiver" range, I_i^k, T_i^k and δm_i^k are ionospheric, tropospheric and multi-path ranging errors, $c \bullet dt$ and $c \bullet \delta$ terms correspond to SV and receiver clock offsets respectively, λN_i^k is the phase ambiguity and ε_i^k is the un-modelled carrier phase noise.

All the terms in Eq. (1) except the last one define the main trend and slow random variations of the phase range between satellite and receiver. The last term ε_i^k can be considered as the sum of un-modeled noises which come from ionospheric phase scintillations, tropospheric phase rapid variations, GNSS satellite oscillator anomalies, GNSS receiver thermal noises, Allan deviation of a GNSS receiver oscillator, vibration-induced phase noises and multipath events.

It is well known that the ionospheric phase scintillations are induced with ionospheric turbulences of hundreds meters—kilometers size which correspond to the Fresnel frequencies from ≈ 0.1 to ≈ 10 Hz (Bhattacharrya et al. 2000). Thus, it is possible to detect such small-scale ionospheric turbulences directly from the noise component $\varepsilon_i^k(1)$ analysis when we use the high sampling rate data (1).

The most convenient approach to extract this noise component from the complex phase ranging data (1) is to use phase derivatives. It allows us to exstract the ε_i^k component directly from the phase measurements without additional processing procedures. One can estimate an instantaneous signal phase value at the phase lock loop (PLL) filter output (at each i-th instant time) based on the discrete Markov's chain model (Kaplan 1996):

$$\varphi_i = \varphi_{i-1} + T_{COR} \cdot \frac{d\varphi_{i-1}}{dt}; \frac{d\varphi_i}{dt} = \frac{d\varphi_{i-1}}{dt} + T_{COR} \cdot \frac{d^2\varphi_{i-1}}{dt^2}; \frac{d^2\varphi_i}{dt^2} = \frac{d^2\varphi_{i-1}}{dt^2} + \xi_{\phi,i-1} \quad (2)$$

where T_{COR} is the PLL pre-detection integration time and $\xi_{\phi,i}$ is the forming zero-mean Gaussian noise of the phase.

First and second components in the Eqs. (2) describe the phase ranging trend and its slow changing. The last component in Eq. (2) is the second-order derivative of the phase which corresponds to the phase noise ε_i^k in (1). At this point, the second order derivative can be suggested as the source of information about the ionospheric scintillations and small-scale ionospheric turbulences in case if the data sampling rate is less or equal to the expected Fresnel frequencies in the scintillation research.

Let us estimate the expected variations of the main components of the phase noise ε_i^k in order to decide if they are small enough to obtain ionospheric phase scintillation reliably. We suppose that the vibration-induced oscillator phase noise is negligible for a stationary GPS receiver. Considering this, the receiver phase noise contains PLL thermal noise and Allan deviation. In case of a third-order phase tracking loop filter the thermal noise standard deviation (SD) σ_T and SD of Allan variance σ_F can be computed from the Eqs. (3) and (4) respectively (Kaplan 1996)

$$\sigma_T = \frac{360}{2 \cdot \pi} \sqrt{\frac{\Delta F_{PLL}}{CN_0} \cdot \left(1 + \frac{1}{2T_{COR} \cdot CN_0}\right)} \quad (3)$$

$$\sigma_F = 160 \cdot \frac{\sigma_F(\tau) \cdot f}{\Delta F_{PLL}} \quad (4)$$

where $\sigma_F(\tau)$ is SD of the short-term Allan variance, ΔF_{PLL} is the PLL noise bandwidth (Hz), CN_0 is carrier-to-noise power ratio in dB*Hz, and f is a signal frequency (Hz).

In general, the thermal noise depends not only on the internal receiver noises but also on the antenna pattern, antenna noise temperature and external noises (the sky noise, the Sun noise and the Earth noise). To simplify, we consider the thermal noise as the zero-mean white noise as it is usually considered for the engineering computations (Kaplan, 1996). In case of stable incoming carrier-to-noise ratio (i.e. CN_0 varies from 30 to 45 dB*Hz) the receiver phase noise level depends on the receiver adjustments and the quality of the receiver reference oscillator. For example, if ΔF_{PLL} = 18 Hz and the receiver oscillator is of good quality (i.e. $\sigma_F(\tau) = 10^{-11}$ or better), then the SD of Allan deviation (σ_F) is negligible and equals to 0.024 rad. However, the value of σ_F

increases dramatically up to 0.22 rad in case of the narrower PLL noise bandpass of ΔF_{PLL} = 2 Hz at the same receiver oscillator quality.

Figure 1 shows SD of the thermal noise (σ_T) versus carrier-to-noise ratio for different sets of receiver adjustments. The value of σ_T does not exceed 0.05 rad in case of correct PLL adjustments and stable level of carrier-to-noise ratio which is higher than 30 dB*Hz (curves 3 and 4, Fig. 1). Reducing of the pre-detection integration time can lead to the corresponding two times increase of σ_T value at the same carrier-to-noise ratio (curves 1 and 2, Fig. 1).

In general, the value σ_T can be kept small enough by means of PLL correct adaptive adjustments even under bad carrier-to-noise ratio. Therefore, the information about ionospheric phase scintillation can be obtained from the second order derivative of the phase in case of both correct PLL adjustments and the short-term Allan variance of $\sigma_F(\tau) = 10^{-11}$ or better.

GNSS satellite clock short-term anomalies can be another serious factor to corrupt pure phase scintillation measurements and bring misleading results to geophysical research. Benton and Mitchel (2012, 2014) observed GPS satellite short-term clock anomalies and found that such events can mimic genuine ionospheric scintillation in the occurrence and time duration. Correspondent SD of such mimicking phase noise can exceed 1.5 radians at both GPS frequencies. The only approach to distinguish and exclude such satellite clock anomalies from the ionospheric scintillation data is to observe the same satellite signal at the observation points located far

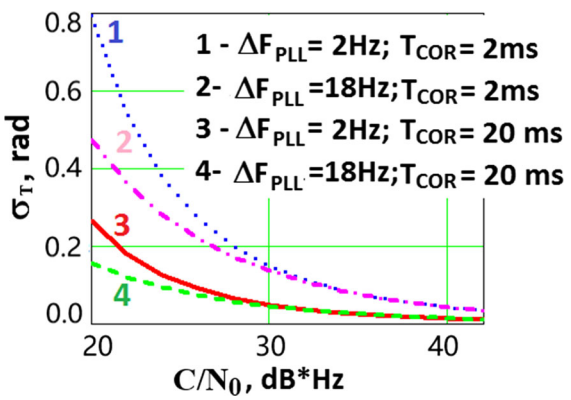

Figure 1
Dependence of GPS receiver thermal noises on carrier-to-noise ratio at PLL input for different receiver adjustments

away from each other (Benton and Mitchel 2014). We follow this recommendation in the present study.

Irregular variations of the tropospheric refractive index can bring additional uncertainty and inaccuracy in the single-frequency observation of the ionospheric phase scintillation. The upper bounds of the tropospheric phase noises SD can be calculated as follows (Gorbunov and Gurvich 1998):

$$\sigma_{TP}^2 = \frac{16\pi^2}{5\lambda^2} \cdot \sigma_n^2 \cdot \Lambda \cdot H_{TP} \cdot \sin^{-1}(\theta) \qquad (5)$$

where λ is the signal wavelength, σ_n is a standard deviation of tropospheric refractive index, Λ is the size of the tropospheric turbulences ($\Lambda_0 < \Lambda \leq \Lambda_m$, where Λ_0 = 10 cm and Λ_m = 1400 m), H_{TP} is the thickness of the tropospheric turbulences layer (H_{TP}= 6–10 km), and θ is the satellite elevation angle.

It is seen that the tropospheric phase variations intensity depends on the refractive index variation and the scale of tropospheric turbulences along the satellite line-of-sight. Thus, we can expect that SD of tropospheric phase noise can vary significantly. Based on a typical values of $\sigma_n = 10^{-6}$, Λ = 100–1400 m and H_{TP} = 6 km the expected upper bounds of σ_{TP} value are calculated as it is shown in Fig. 2. SD of the tropospheric phase noise mostly does not exceed 0.1 rad for satellites that are at the elevation angles > 40°.

In order to separate the tropospheric and ionospheric effects one of the possible means is to compare time scale of the phase variations taking in account the following condition:

$$\Delta T \approx \Lambda_m \cdot V_d^{-1} \approx \Lambda_m \cdot (V_{db} + V_{SV}\cos(\alpha)) \qquad (6)$$

where ΔT is the time period of the phase noise variations as a result of intersection between the ionospheric (or tropospheric) turbulence and satellite line-of sight, Λ_m is the maximum size of the turbulence, V_d is the relative speed between the turbulence (which travels with the speed of V_{db}) and the satellite line-of-sight speed (V_{SV}) at the troposphere (or ionosphere) altitude, α is an angle between the ionospheric (tropospheric) turbulence drift direction and the direction of SV trajectory (α = 0–360°).

The speed V_{SV} is not higher than 70–80 m/s (depending on the elevation angle) at the ionospheric altitudes. This speed is comparable with the speed of

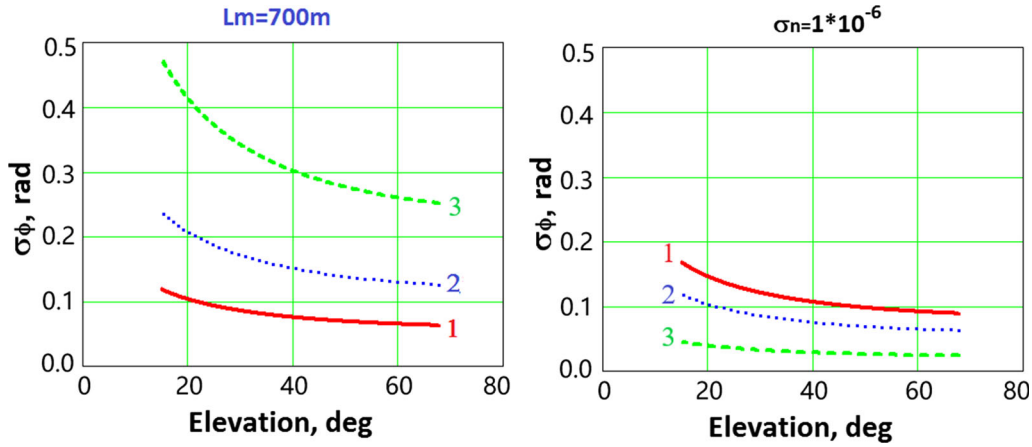

Figure 2
Dependence of tropospheric phase noise on satellite elevation. Left panel: $\sigma_n = 10^{-6}$ (curve 1), $\sigma_n = 2 \times 10^{-6}$ (curve 2) and $\sigma_n = 4 \times 10^{-6}$ (curve 3) for the turbulence size $\Lambda = 700$ m; Right panel: $\Lambda = 100$ m (curve 3), $\Lambda = 700$ m (curve 2) and $\Lambda = 1400$ m (curve 1) for the turbulence intensity $\sigma_n = 10^{-6}$

traveling tropospheric turbulences but it is much smaller if compare to the speed of ionospheric plasma turbulences drift. For example, if $\Lambda_m = 1400$ m, $V_d = 200$ m/s and $\alpha = 0$ for tropospheric turbulence, then the duration of the correspondent tropospheric phase noise disturbance will be about 7 s. The speed of the ionospheric disturbances drift varies in a very wide range: from 200 to 3000 m/s (Matsumura et al. 2011; Tsugawa et al. 2011). Let us assume $\Lambda_m = 20$ km for the ionosphere, then it will yield the duration of the ionospheric phase scintillation which will be from 7 to 100. Thus, the expected time duration of the ionospheric and tropospheric phase noise variations should differ from each other significantly. However, the above mentioned criterion does not work reliably in case of "cloud of turbulences". In this case the only approach to separate the weak ionospheric and strong tropospheric scintillations is to combine double-frequency phase ranging.

The ionospheric scintillations component of the phase noise can be defined as zero-mean Gaussian noise with standard deviation of $\sigma_{\hat{\phi}}$ (Afanasiev et al. 2001; Kolesnik et al. 2002) as follows:

$$\sigma_{\hat{\phi}}^2 = \frac{1}{2 \cdot d_1^2} \cdot (\sigma_{in}^2)^2 + \frac{1}{d_1 \cdot d_2} \cdot (\sigma_{io}^2)^2 + \frac{1}{2 \cdot d_2^2} \cdot (\sigma_{out}^2)^2 + \sigma_{\tilde{\phi}}^2 \tag{7}$$

where $\sigma_{\tilde{\phi}}$ is the SD of the phase variations due to the signal scattering from the small-scale ionospheric turbulences, σ_{in}, σ_{io} and σ_{out} are SDs of the ionospheric phase variations as a result of the wave trajectory jitter due to the influence of turbulences before, during and after the signal passed through the layer, and d_1, d_2 are distances between the receiver and the layer and between the layer and SV.

The $\sigma_{\tilde{\phi}}$, σ_{in}, σ_{io} and σ_{out} values depend on the parameters of the ionospheric turbulences. In the simplest case (when there is only one "averaged" turbulence of fixed size and intensity) this dependence can be defined as follows (Afanasiev et al. 2002; Kolesnik et al. 2002):

$$\sigma_{in}^2 \approx \frac{\sqrt{\pi} \cdot L \cdot d_1^2}{4(d_1 + d_2 + L)^2} \cdot \left(\frac{L^2}{3} + d_2 \cdot (L + d_2) \right) \cdot \frac{\sigma_i^2}{l_i} \tag{8}$$

$$\sigma_{io}^2 \approx \frac{\sqrt{\pi} \cdot L d_1 d_2}{4(d_1 + d_2 + L)^2} \cdot \left(\frac{L}{2}(d_1 + d_2) + \frac{L^2}{6} + d_1 d_2 \right) \cdot \frac{\sigma_i^2}{l_i} \tag{9}$$

$$\sigma_{out}^2 \approx \frac{\sqrt{\pi} \cdot L \cdot d_2^2}{4(d_1 + d_2 + L)^2} \cdot \left(\frac{L^2}{3} + d_1 \cdot (L + d_1) \right) \cdot \frac{\sigma_i^2}{l_i} \tag{10}$$

$$\sigma_{\tilde{\phi}}^2 \approx \frac{\sqrt{\pi}\cdot L}{2}\cdot \sigma_i^2 \cdot l_i \tag{11}$$

$$\sigma_i^2 = LZ\cdot\frac{0.066\cdot C_{\tilde{\varepsilon}}^2}{l_i\cdot\Gamma(p)} \cdot\left(l_i^2-\frac{1}{k_m^2}\right)^{p-1}\times\exp\left(\frac{k_0^2}{k_m^2}-k_0^2\cdot l_i^2\right) \tag{12}$$

where L and Z are the ionospheric F-layer thickness and length respectively (the irregularity layer extends from $Z = 0$ to $Z = L$), $\Gamma(p)$ is Gamma—function of p, p is the degree of the wave number in the ionospheric turbulence power-low spectra (p value varies from 2 to 4 for the ionosphere), C_{ε} represents the intensity of the ionospheric turbulences, l_i is the size of the turbulences inside the F-layer, and $k_0 = 2\pi/l_{\max}$, $k_m = 5.92/l_{\min}$ are the spatial wave numbers.

Here, we consider the ionospheric irregularities that are about of the first Fresnel zone size or larger. This is the case of the geometrical optics assumption. The formulas (8)–(12) are obtained under the assumption that the transverse size equal to the lengthwise size. The increase of the anisotropy factor results in the square root increase of the phase fluctuations (as the first approximation). It is correct enough while geometrical optics condition is fulfilled.

Figure 3 shows the modeled $\sigma_{\hat{\phi}}$ values with respect to elevation angle for several probable sets of the ionospheric turbulence parameters. For a moderate small-scale turbulence the $\sigma_{\hat{\phi}}$ value mostly does not exceed 0.5 rad for satellites at elevation angles $> 40°$ (Fig. 3). In case of strong ionospheric turbulences the phase noise SD can be significantly higher. It worth noting that the above mentioned calculation is simplified and does not take into account the low power turbulences spectrum as well as the multiple scattering events in the thick layer of the intense ionospheric turbulences. In the case of the mentioned impact the expected $\sigma_{\hat{\phi}}$ value can be several times higher at the same elevation angles (Bhattacharrya 2000).

Therefore, we can calculate the modeled $\frac{d^2\phi_i}{dt^2}$ values for two cases: (1) there are impacts of all the noises components (Eqs. 3–5) except the impact of ionospheric scintillations; (2) there is only ionospheric scintillations impact (Eq. 7–12). The modeled phase range time series can be described by Eq (13) for the first case and by Eqs. (14) for the second case

$$\Phi 1(\theta,t) = \rho(t) + \delta T(\theta,t,\sigma_{TP}) + \delta R(t, CN_0, \sigma_T, \sigma_F) \tag{13}$$

$$\Phi 2(\theta,t) = \rho(t) - \delta I(\theta,t,\sigma_{\varphi}^{-}) \tag{14}$$

where: $\rho(t)$ is the geometric range, $\delta T(\ldots)$ is the tropospheric zero-mean Gaussian noise with standard deviation—σ_{TP} (5), $\delta R(\ldots)$ is zero-mean Gaussian noise due to Allan short term deviation and thermal noises, CN_0, σ_T, and σ_F are the terms which were described in Eqs. 3–4, and $\delta I(\ldots)$ is the ionospheric zero-mean Gaussian phase noise which SD equals to $\sigma_{\hat{\phi}}$ (Eqs. 7–12).

Figure 4 illustrates the results of modeling for both Model 1 (Eq. 13, panel A) and Model 2 (Eq. 14, panel B). Geometric phase ranging ($\rho(t)$) and elevation for satellite PRN 14 at ISTP station (Irkutsk, Russia, geographic coordinates 52° N, 104° E) were used to reconstruct the model time series from Eqs. (13) and (14) at 50 Hz time resolution.

To model these time series (Fig. 4) the moderate tropospheric and ionospheric turbulences were supposed to be present with the following parameters: Λ = 700 m and $\sigma_n = 10^{-6}$ for the tropospheric turbulence, $N_0 = 10^{12}$ el/m^3, $\Delta N/N_0 = 5\%$ and l_i = 5 km for the ionospheric turbulence. Good quality of the GPS receiver hardware (CN_0= 40 dB Hz, σ_T = 0.014 rad, and σ_F = 0.024 rad) was assumed as well. In addition, the short-term satellite reference oscillator instability was neglected as the short-term Allan variance is usually 10^{-11} or better. Multipath phase noise was ignored in modeling process as well.

Figure 4 shows that the modeled $\frac{d^2\phi_i}{dt^2}$ ionospheric variations (Eq. 14, Fig. 4b) are significantly higher than the other error sources impact (Eq. 13, Fig. 4a). This sounds promising for the $\frac{d^2\phi_i}{dt^2}$ use to detect ionospheric phase scintillation in case of moderate tropospheric disturbances and good quality of GPS receiver. In contrast, to the first order derivative (middle panels of Fig. 4), the second-order phase derivative does not contain both the trend due to SV motion and ambiguity. Consequently, the $\frac{d^2\phi_i}{dt^2}$ parameter can be considered as an easy-derived and promising index to detect small-scale ionospheric turbulences.

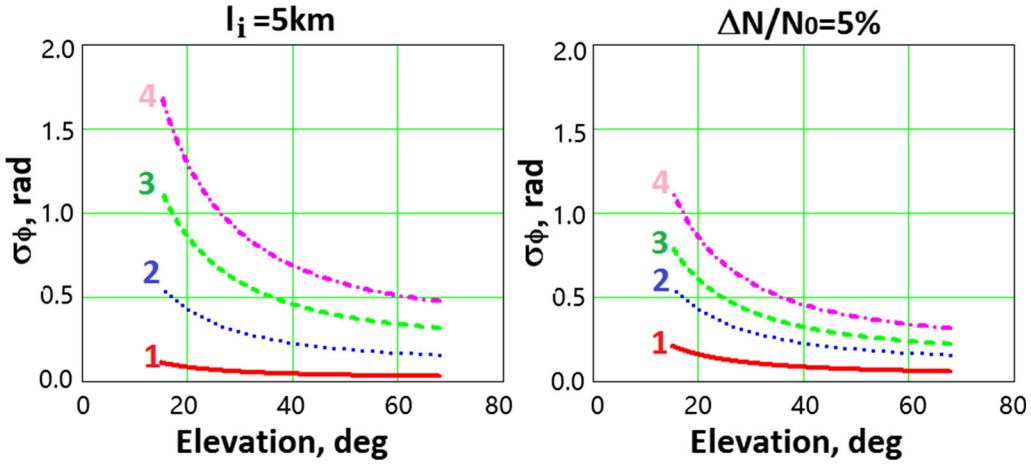

Figure 3
Dependence of ionospheric phase noise on satellite elevation. Left panel: $\Delta N/N_0 = 1\%$ (curve 1), $\Delta N/N_0 = 5\%$ (curve 2), $\Delta N/N_0 = 10\%$ (curve 3) and $\Delta N/N_0 = 15\%$ (curve 4) for the turbulence size $l_i = 5$ km. Right panel: l_i = 100 m (curve 1), l_i = 5 km (curve 2), l_i = 10 km (curve 3) and l_i = 20 km (curve 4) for the turbulence intensity $\Delta N/N_0 = 5\%$. The background is $N_0 = 10^{12}$ el/m^3 for all the cases

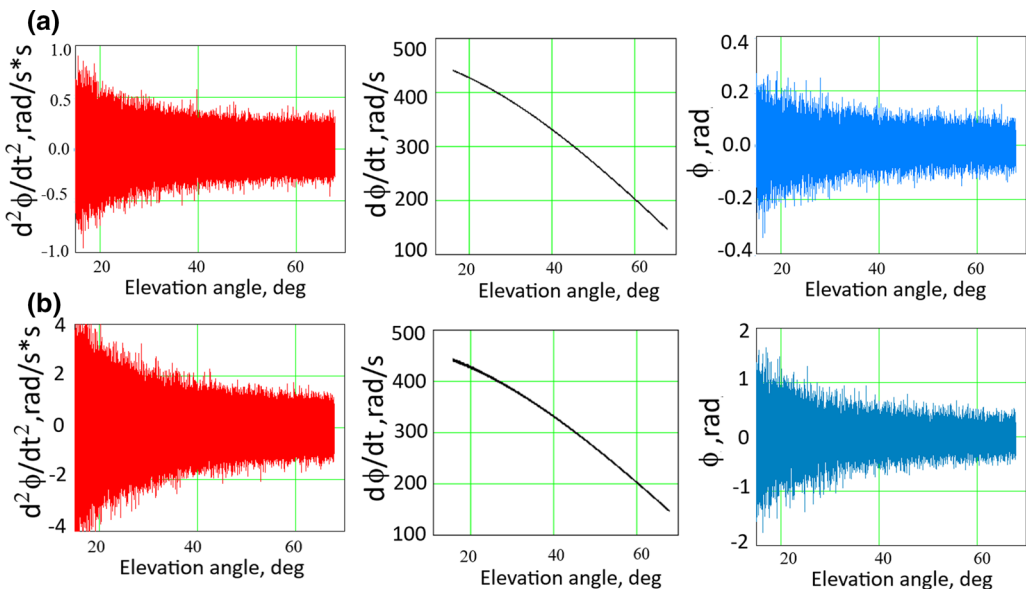

Figure 4
Results of phase noise modeling according to Eqs. 13 (**a**), and 14 (**b**)

3. *Experimental Results and Analysis*

3.1. *Experiment Environment and Data Sources*

The second order of GPS carrier phase time series were measured under the geomagnetic storm conditions to test and prove our hypothesis. Comparative analysis of efficiency of the main ionospheric indices and the second-order phase derivative parameter was conducted in the above mentioned conditions as well. In the present study all the necessary ionospheric parameters and indices such as TEC, ROTI, DROTI, *S4* and $\sigma\varphi$, as well as the carrier-to-noise ratio (*C/N0*) and the second-order derivative of the GPS carrier phase were derived from the 50 Hz *L1* and *L2* GPS data. These data (Yasyukevich 2017) were obtained

at the mid-latitude station ISTP (Irkutsk, Russia, geographic coordinates 52°N, 104°E) equipped with JAVAD GNSS receiver. The station is a part of SibNet network (Yasyukevich et al. 2018)

To verify the results additional GPS L1 50 Hz data obtained from EDMC station (Canada, geographic coordinates 53°N, 113°W) equipped with SEPTENTRIO PolaRxS GNSS receiver (Bougard et al. 2011) were involved (Jayachandran et al. 2009). These data was available in the specific non-RINEX format (PolaRxS SBF Reference Guide) as follows: GPS time of week (s); SV identification number; Signal type; *L1* (or *L2*) Carrier phase (cycles); signal in-phase (*I*) and quadrature (Q) components (dimensionless). Not all of the data obtained from EDMC station contained *L2* carrier phase measurements. That is why we compared our results for *L1* data only. Carrier-to-noise ratio (CNR) was computed based on the above mentioned specific data in terms of carrier-to-noise ratio (dBW) as follows (Tiwari and Strangeways 2015):

$$CNR = 10 \cdot lg\left(\frac{WBP}{n} - 1\right) \tag{15}$$

$$WBP = \sum_{i=1}^{N} (I_i)^2 + (Q_i)^2 \tag{16}$$

where n is the noise term at PLL input that is defined based on the model

$$n = \frac{1}{k} \cdot \left(\frac{a}{sin(\gamma \cdot b + c)}\right) \tag{17}$$

where a = 51.94, b = 0.0093 and c = 0.7305 are the noise term model parameters; γ is a satellite elevation angle; the coefficient "k" is obtained before the experiment by leveling the *CNR* value (15) with the ideal C*NR** value depending on the elevation angle.

The CNR* value is defined based on the known technical standards (IS-GPS-200J 2018) as follows

$$CNR* = P_{rec} + G_A - N_T - L_{tr} - L_{dg} \tag{18}$$

where *Prec* is the signal level at the receiving point (dBW); G_A is the antenna gain (dB); N_T is the spectral density of the receiver thermal noise power (dBW); L_{tr} is the total power loss during filtering, frequency conversion and the signal attenuation in the cable (dB); L_{dg} is the signal power loss due to its analog-to-digital conversion (dB). The typical values *Prec* (depending on elevation angle), G_A (depending on elevation angle), N_T, L_{tr} and L_{dg} were obtained from (IS-GPS-200J, 2018; Kaplan 1996).

As the de-trended TEC data is used to calculate ROTI and DROTI indices the un-calibrated code-levelled phase TEC time series was derived from GPS phase and code measurements for this study. The phase TEC time series were de-trended by centered moving average with 30 s accumulation time. *DROTI* values were calculated from the de-trended 50 Hz TEC data with 1 s time resolution. The scintillation indices (*S4* and $\sigma\varphi$) were calculated from the de-trended 50 Hz *L1* data based on standard procedure (Van Dierendonck et al. 1993) also with 1 s resolution.

It is known that geomagnetic storms can cause ionospheric disturbances including the small-scale disturbances which are of our particular interest in this research. The period of the intense storm of June 22, 2015 was chosen for the analysis. Figure 5 shows Kp and Dst indices variations during June 21–23, 2015. Three sudden storm commencements (SSC) caused by the interplanetary shocks occurred at 16:46 UT on June 21st, 05:47 and 18:30 UT on June 22nd (Piersanti et al. 2017; De la Luz et al. 2018). After the last SSC the main phase (MP) of the geomagnetic storm (Dstmin = − 204 nT) developed (June 22–23). The recovery phase (RP) lasted the next days (June 23–July 1). The highest Kp values were observed during MP. Thus, geomagnetic background was disturbed during all the days illustrated in Fig. 5.

The Kp and Dst indices data were obtained from the OMNIweb database (https://omniweb.gsfc.nasa.gov/form/dx1.html, last access: January 29, 2018).

3.2. *Comparative Analysis of Efficiency of the Main Ionospheric Indices*

The behavior of the $\frac{d^2\phi_i}{dt^2}$ parameter was compared to standard ionospheric scintillation indices such as *DROTI*, *S4* and $\sigma\varphi$ under June 22, 2015 geomagnetic storm conditions. According to (Bhattacharya 2000), the relationship between *S4*, $\sigma\varphi$ and *DROTI* indices is complex, but in most cases the *S4* increase means *DROTI* increase and vice versa. Figure 6 shows variations of $\frac{d^2\phi_i}{dt^2}$, *DROTI*, *S4* and $\sigma\varphi$ indices

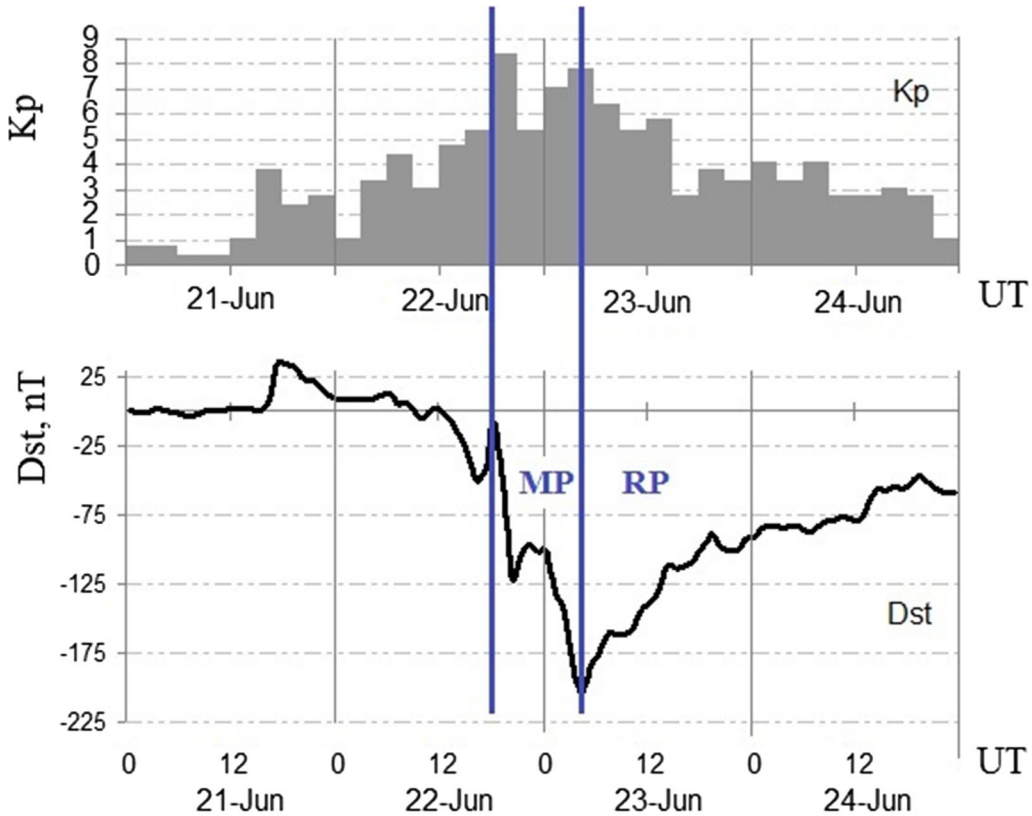

Figure 5
Kp (upper panel) and Dst (lower panel) variations during June 21–24, 2015. The moments of MP and RP are indicated with the vertical lines

during the storm for the GPS satellites PRN 06, PRN 15 and PRN 27.

Good similarity between $\frac{d^2\phi_i}{dt^2}$ and $\sigma\varphi$ variations is seen for all the scintillation events and for all the satellites under consideration (Fig. 6b, c). Nevertheless, the peaks of $\frac{d^2\phi_i}{dt^2}$ are pronounced more sharply. The similarity between the $\frac{d^2\phi_i}{dt^2}$ and *S4* variations is worse. There is a general similarity in variations of two parameters, but *S4* values are rather noisy and contain several peaks which do not coincide in time with $\frac{d^2\phi_i}{dt^2}$ variations (Fig. 6b, d).

The worst similarity is between $\frac{d^2\phi_i}{dt^2}$ and *DROTI* for all the cases under consideration (Fig. 6b, e): the form of *DROTI* variations envelope significantly differs from the $\frac{d^2\phi_i}{dt^2}$ variations envelope. To add, DROTI observations are rather noisy. Almost no *DROTI* response is seen for the SV PRN 27 (Fig. 6e, middle panel). As noticed before, the small-scale ionospheric turbulences do not provoke significant TEC response. Consequently, even weaker response can be expected in TEC-derived indices as DROTI, which is probably the case of Fig. 6e.

Based on Fig. 6 results we can point out some advantages of $\frac{d^2\phi_i}{dt^2}$ index as follows: (a) $\frac{d^2\phi_i}{dt^2}$ response to small-scale turbulences is more sharp and exact in time than the responses of other scintillation indices; (b) measurements at only one (single) GPS frequency are needed to calculate $\frac{d^2\phi_i}{dt^2}$ parameter in contrast to TEC and TEC-based indices; (c) being based on single-frequency data the $\frac{d^2\phi_i}{dt^2}$ index avoids possible impact from additional inter-frequency noises and *L1*-aiding technique features (McCaffrey et al. 2018); (d) the second-order derivative of the carrier phase is calculated directly from the high-rate *L1* or *L2* phase data in contrast to typical scintillation indices which require additional pre-processing and depend on the features of the data processing technique.

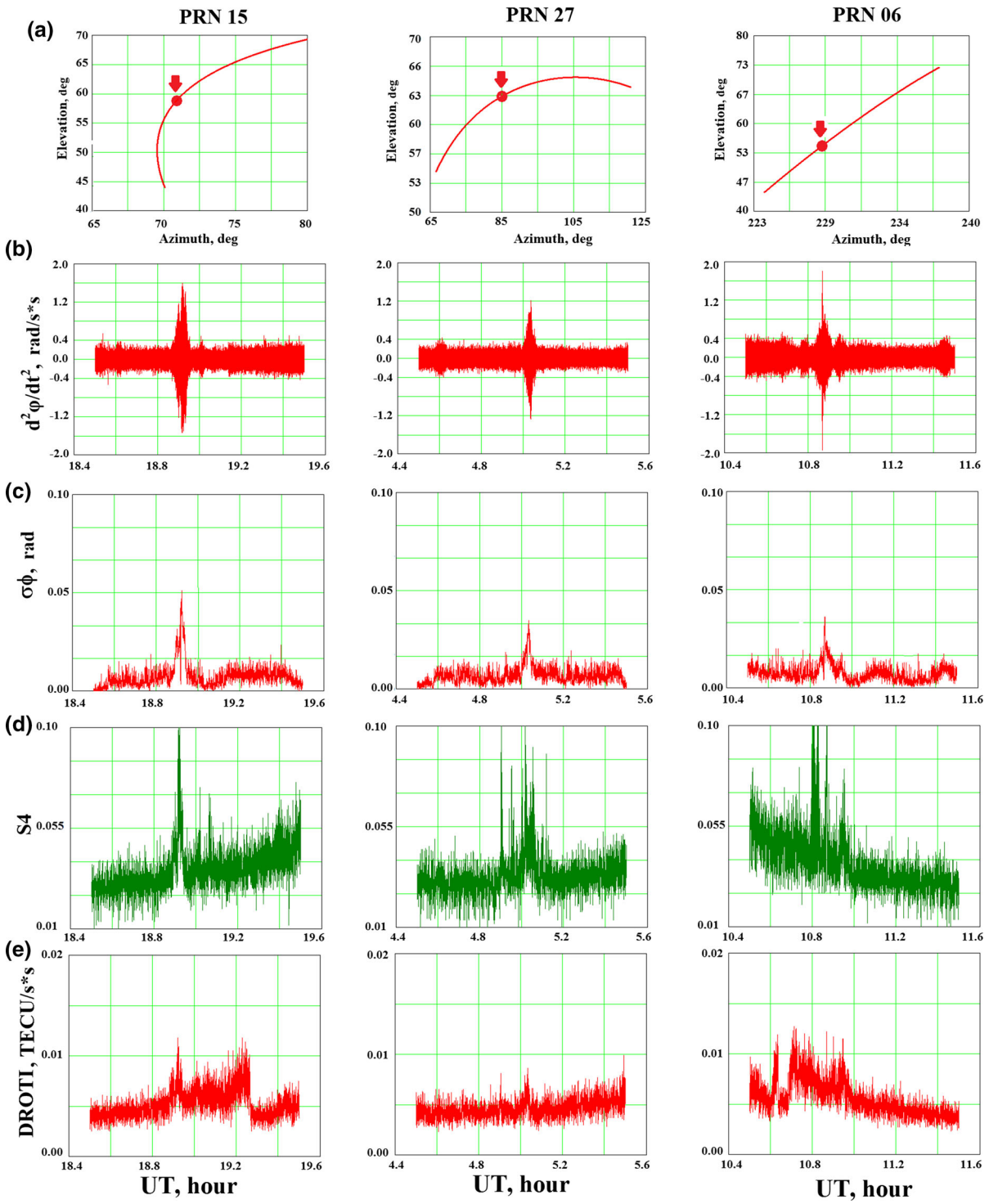

Figure 6
Comparison between the $\frac{d^2\phi_i}{dt^2}$ parameter and main ionospheric scintillation indices. The dots indicate the approximate SV angular positions when the scintillation events were observed in $\frac{d^2\phi_i}{dt^2}$ time series

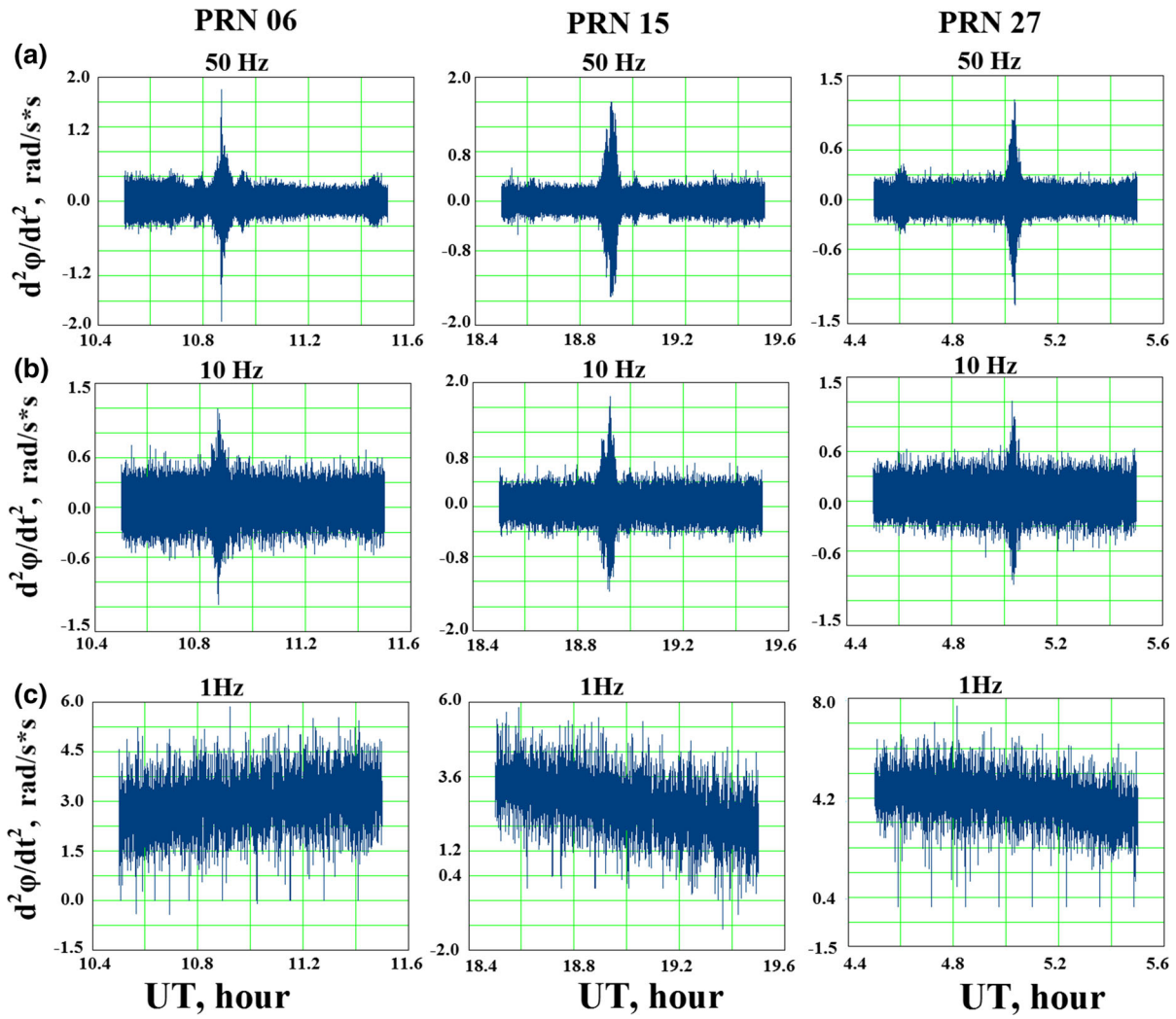

Figure 7
The phase second-order derivative time series in case of 50 Hz data time-rate (**a**), 10 Hz data time-rate (**b**) and 1 Hz data time-rate (**c**) for PRN 06, PRN 15 and PRN 27 on June 22, 2015 at ISTP station

3.3. The Data Sampling Rate

Time resolution of the phase ranging data is considered to be a crucial parameter in the ionospheric scintillation research. For example, Jacobsen (2014) showed significant sampling rate effect on ROTI estimation. Indeed, the minimal size of the ionospheric irregularities of refractive origin is about the first Fresnel-zone sized (300–400 m). Such irregularities still can cause both refractive and diffractive variations not only in the phase ranging data but also in other ionospheric parameters such as TEC and its derivatives, *S4* and $\sigma\varphi$ which are calculated with corresponding time resolution. Ionospheric scintillations induced with the first Fresnel-zone sized irregularities can be observed within $\approx$ 0.1–10 Hz frequency band. Smaller irregularities (from tens of meters to 100–300 m) are mostly considered to provoke diffractive amplitude and phase variations. In order to detect such small scale ionospheric irregularities as high time rate data as possible is needed (McCaffrey and Jayachandran 2017).

Diffractive phenomena provoke phase scintillations and can be detected with $\sigma\varphi$ index. *S4* also can

be useful in this case as phase scintillations of diffractive origin are usually accompanied with severe amplitude fluctuations. In turn, scintillations of refractive origin can be detected with both scintillation indices and also with sharp TEC variations. Therefore, *ROTI, DROTI* (Pi et al. 1997; Bhattacharrya 2000) or sDPR index (Ghoddousi-Fard et al. 2013; Prikryl et al. 2016; Priyadarshi et al. 2018) can be used to detect ionospheric scintillations of refractive origin.

Several km size irregularities mostly cause ionospheric scintillations of refractive origin. When such irregularities dominate, *S4* does not vary significantly and almost has no correlation to *ROTI, DROTI*, and even to $\sigma\varphi$. In case of predominance of the diffractive first-Fresnel zone sized irregularities, carrier-to-noise ratio (CNR) or *S4* should vary significantly and usually show high correlation with $\sigma\varphi$ variations. (Bhattacharrya 2000).

Irregularities of different scales can be present in the ionosphere simultaneously, for example when volcanic eruptions, powerful explosions, rocket launching or other triggering phenomena occur under disturbed geomagnetic conditions. In this mixed case all the ionospheric indices will be partly correlated with each other. In addition, ionospheric irregularities can move with quiet different velocities and directions. The use of 1 Hz or lower time resolution does not allow to understand if the ionospheric event was induced with diffractive irregularities of hundreds meters or with larger ionospheric irregularities of tens of kilometers. We suggest that the high resolution 50 Hz (or higher) data solves this problem if there is no irregular variations of the thermal noise or short term instability of reference oscillator. We do not consider the case of irregular background noise fluctuations. We suppose that such noise fluctuations will bring the similar response in all the carrier phase measurements for all the satellites in view simultaneously. Thus, it will be easy to interpret such simultaneous and similar events and exclude them from further consideration.

To test our assumption we compare 1 Hz, 10 Hz and 50 Hz $\frac{d^2\phi_i}{dt^2}$ time series for the same events and under the same geomagnetic storm conditions. Figure 7 shows the results of comparison for PRN 06, PRN15 and PRN27 on June 22, 2015.

For all three satellites the $\frac{d^2\phi_i}{dt^2}$ values obtained from 1 Hz GPS data do not reflect any event (Fig. 7c). The $\frac{d^2\phi_i}{dt^2}$ values obtained from 10 Hz data show clear peaks (Fig. 7b). The peaks of 50 Hz $\frac{d^2\phi_i}{dt^2}$ variations are even more pronounced. It should be emphasized that 1 Hz data shows the significant noise level and additional regular trend, which are absent or almost absent in the higher rate data. In case of the highest data rate (50 Hz) the background $\frac{d^2\phi_i}{dt^2}$ values do not exceed 0.4 rad/s s and there is no regular trend (Fig. 7a). For lower data rate (10 Hz) a weak regular trend appears in the $\frac{d^2\phi_i}{dt^2}$ time series, and background noise increases up to 0.6 rad/s*s. The $\frac{d^2\phi_i}{dt^2}$ values increase 4–5 times and exceed 2–3 rad/s s for 1 Hz data (Fig. 7c). This result can be considered at the standpoint of the potential resolution of the GNSS radio-sounding methods in the ionospheric research and it even needs to be enhanced in special studies like (McCaffrey et al. 2017).

3.4. Multipath and Blocked Signal Effects

The next step of our testing is to verify that the scintillation events revealed above were not connected to the multipath and/or blocked signal effects. It is not always possible to distinguish the pure ionospheric scintillation event and the multipath induced event. The majority of the multipath-induced fluctuations are observed at lower elevation angles. However, it is also not a thorough determination of multipath as it is possible to observe it at the higher elevations as well. The main selection criteria to identity the multipath event are regular time shift between the peaks of the phase variations which repeats day by day and the regular time drift of the whole multipath pattern at the receiving point. Both the time shift and the form the multipath pattern may vary from 1 day to another due to radio propagation environment changes. But the time shift between the certain points of the multipath pattern should be approximately equal or more than the regular sidereal day offset. This offset is taken to be − 235.91 s (3.9 min) from the 24 h mean solar day (Hofmann-Wellenhof et al. 2008). The time drift of the whole multipath pattern for a particular satellite should have the same direction from one day to another.

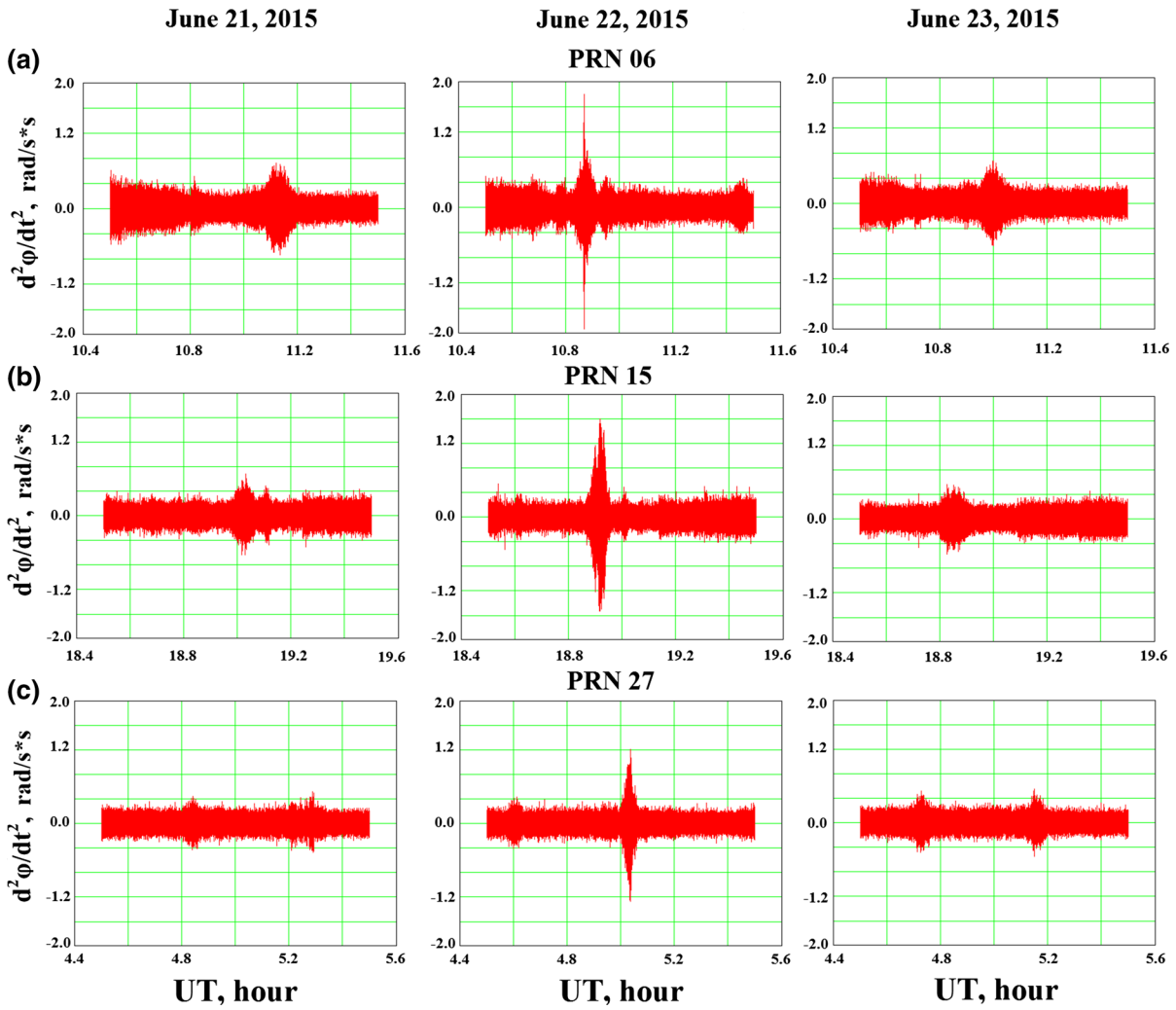

Figure 8
The $\frac{d^2\phi_i}{dt^2}$ time series during three consequent days on June 21–23, 2015 for satellites. PRN06 (**a**), PRN15 (**b**), PRN27 (**c**)

Figure 8 illustrates $\frac{d^2\phi_i}{dt^2}$ variations deduced from 50 Hz data on June 21, June 22 and June 23, 2015 for three satellites PRN 06 (panel a), PRN 15 (panel b) and PRN 27 (panel c). There were no significant local peaks in the $\frac{d^2\phi_i}{dt^2}$ variations on June 21 and June 23. In contrast there are sharp and rapid variations of $\frac{d^2\phi_i}{dt^2}$ on June 22, 2015 for all the satellites. On the other hand, there are some smaller peaks in the $\frac{d^2\phi_i}{dt^2}$ variations for satellites 06 and 15 on June 21 and June 23 (Fig. 8, panels a and b). It is seen that there is no regular time shift and there is no regular time drift of the multipath pattern from day to day for these satellites. Based on this, we can suggest that the events in Fig. 8 do not have the multipath-induced origin.

As an example of the multipath or blocked signal effects Fig. 9 presents the $\frac{d^2\phi_i}{dt^2}$ variations for PRN 24 obtained at ISTP station on the same three consequent days. Two important facts should be stressed here. First, the $\frac{d^2\phi_i}{dt^2}$ variations during three consequent days are characterized by the very similar envelope form, especially on June 21 and 22 (Fig. 9a, b, left). Second, the time shift between the $\frac{d^2\phi_i}{dt^2}$ peaks, marked with pointers, on the considered days is about 5–6 min. And, finally the time drift of the whole multipath pattern has the same direction during these three consequent days. This allows us to consider the event in Fig. 9 to be a multipath or blocked signal effect.

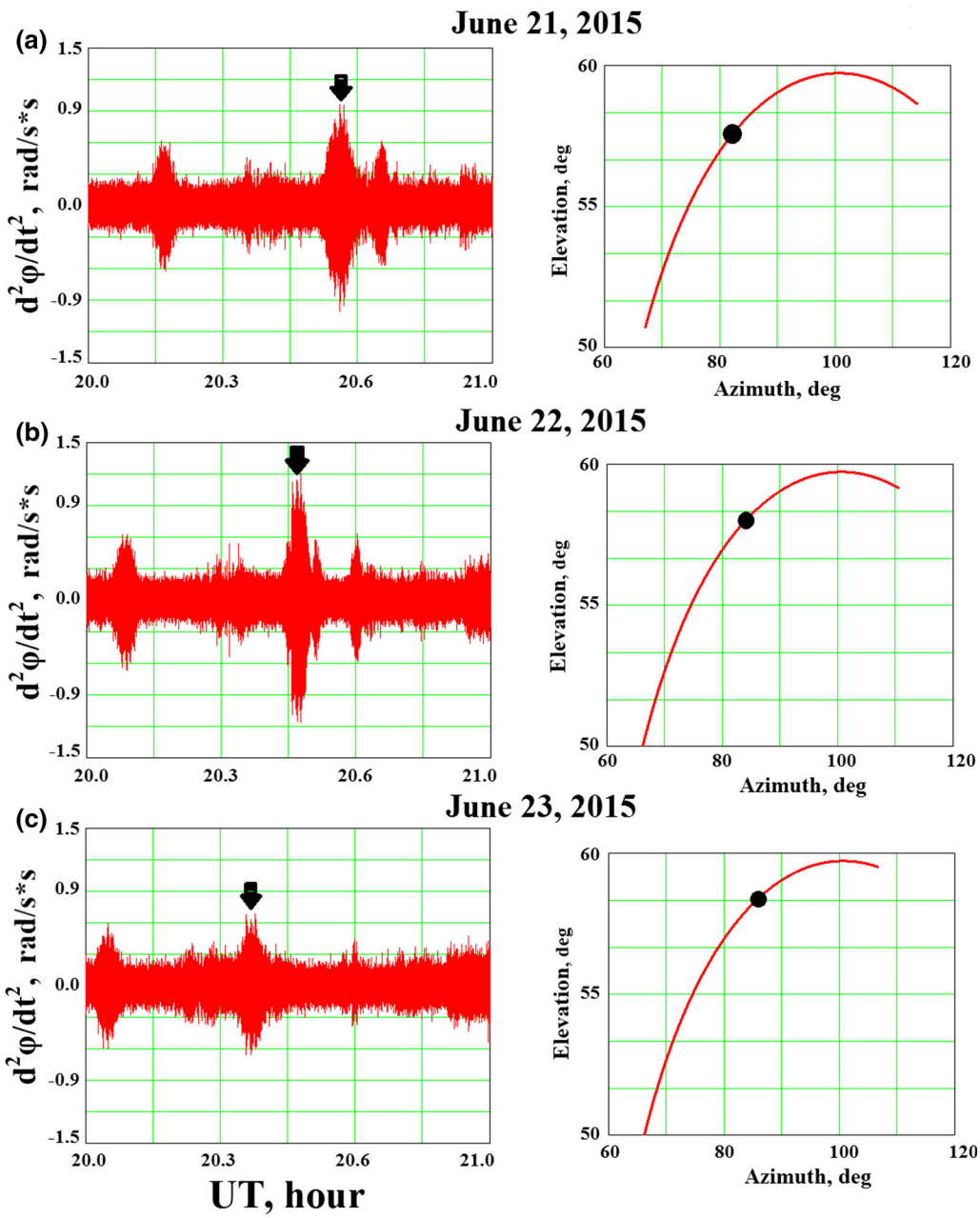

Figure 9
An example of the multipath or blocked signal effects for PRN 24 at ISTP during June 21–23, 2015. Dots and pointers indicate maximal peaks in the $\frac{d^2\phi_i}{dt^2}$ variations (left) and the moments of corresponding SV angular position (right)

The same analysis performed for the cases illustrated in Fig. 8 unfolds nothing of the kind. It allows us to consider the events in Fig. 8 to be exactly the ionospheric scintillations revealed with the second-order derivative of the GPS signal carrier phase.

3.5. *Excluding the Impact of Satellite Clock Short-Term Anomalies Events*

It is necessary to be sure that the scintillation events under our consideration have nothing to do with the other probable sources of the scintillation

"mimicking" events. The satellite reference oscillator can bring such "mimicking" events due to the reference oscillator short term instability. Such "mimicking" events were found first by (Benton and Mitchell 2012). According to (Benton and Mitchell 2014), there is an easy way to distinguish the similar events as the reference oscillator-induced. This way is the synchronous measurements of the carrier phase from the same satellite by widely spaced receivers. This method works in the case if there are no ionospheric scintillations, multipath events and short-term variations in the receiver clock at both of the receiving points at the same time.

We can not control all the factors at two widely spaced receivers. On the other hand it is unlikely that all the factors could happen at two widely separated receivers at the same time. In contrast, we are certain that the satellite clock short-term anomaly event, if occurs, brings the similar synchronous responce to the carrier phase measurements which were obtained from two widely spaced receivers. For this purpose we involved the 50 Hz *L1* data from EDMC station in Canada (Jayachandran et al. 2009) for June 22, 2015. Unfortunately, some data was not available for the comparison because the satellites PRN06 and PRN 27 were out of view at EDMC site between 10 UT and 12 UT and between 04 UT and 06 UT respectively.

Figure 10 shows that there no synchronous responces in the carrier phase measurements obtained from the satellite PRN 15 at both reception points ISTP and EDMC. These receivers are widely spaced and work under different conditions. There is an obvious scintillation event at $\sim$ 18.90 UT at ISTP site (as it was discussed earlier) and there is the short event at 18.60 UT at EDMC site (Fig. 10, panel b). Probably, the last one is the multipath-induced event due to the low elevation angle (Fig. 10, panel a, left). Both events obtained at ISTP and EDMC sites were accompanied with the sharp fading of carrier-to-noise ratio (Fig. 10, panel c). Based on the said above, Fig. 10 does not prove that the event at $\sim$ 18.90 UT (at ISTP site) is the satellite clock short-term anomaly event.

Regardless to the lower elevation angle of the satellite PRN 15 at EDMC, the level of the phase noise was much lower in comparison to the level at ISTP (Fig. 10b). This allows us to imply the better quality of the reference oscillator of SEPTENTRIO receiver in comparison to JAVAD receiver. The overall comparison of data from two sites yields the clear conclusion that the phase scintillation events revealed for PRN 15 are not connected with satellite clock short-term anomaly.

Another conclusion by (Benton and Mitchell 2014) was that all the above mentioned "mimicking" events related to the block IIR vehicles, with rubidium oscillators. They were launched in 1997 and 1999, respectively, and are now substantially beyond their design lifetimes. There were satellites Navstar 43 (PRN13), Navstar 46 (PRN 11), Navstar 2A-13 (PRN 30) and satellite GPS IIF SV-2 satellite (PRN 01) that brought scintillation "mimicking" events. All these satellites were out of our consideration in the manuscript. Hence, we think that the scintillation events under our consideration are not related to the satellite-induced anomalies and scintillation "mimicking" events.

4. Conclusions

In the present study, the second-order derivative of the GPS signal phase is suggested and proved as a promising means to detect small-scale ionospheric irregularities. It was found that 50 Hz data sampling rate is an adequate time resolution for the ionosphere diagnostics purposes sufficient to reveal small-scale irregularities which are responsible for the ionospheric scintillations. The hypothesis of possible $\frac{d^2\phi_i}{dt^2}$ parameter use for ionospheric scintillations detection was tested, The experimental and modeling results proved the hypothesis. The period of the intense geomagnetic storm was chosen for the experimental analysis because geomagnetic disturbances are the most probable scintillation trigger at mid-latitudes.

The bounds of the main components of the phase noise were estimated in order to decide if they are small enough to detect and monitor the ionospheric phase scintillations from the complex single-frequency carrier phase time series by means of its second order differencing. In order to achieve adequate reliability and sensitivity of the $\frac{d^2\phi_i}{dt^2}$ parameter as an indicator of small-scale weak ionospheric

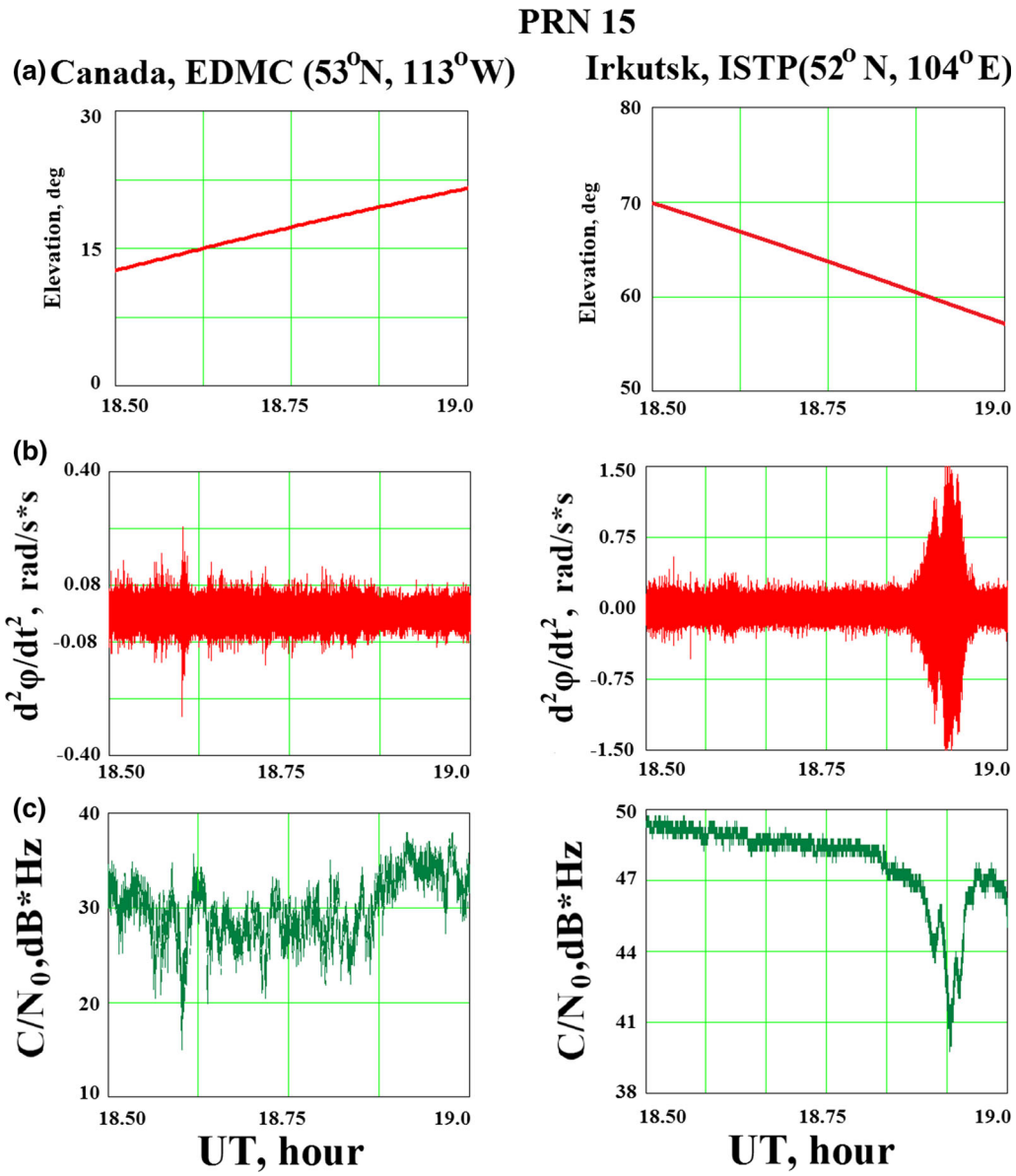

Figure 10
Comparison between the $\frac{d^2\phi_i}{dt^2}$ time series derived from the synchronic *L1* measurements at two widely separated sites ISTP (right) and EDMC (left) for PRN 15 on June 22, 2015

disturbances some additional conditions should be taken into account.

1. PLL thermal noise should be kept small enough by means of PLL correct adaptive adjustments and short-term Allan variance should be $\sigma_F(\tau) = 10^{-11}$ or better.
2. The results of modeling proved that moderate tropospheric disturbances do not limit the $\frac{d^2\phi_i}{dt^2}$ index use as an indicator of the ionospheric scintillations. In case of strong tropospheric disturbances, however, additional testing of the $\frac{d^2\phi_i}{dt^2}$ index is needed.
3. It was shown that the sensitivity of $\frac{d^2\phi_i}{dt^2}$ parameter crucially depends on the data sampling rate. The

higher sampling rate provides more clear and more intense peaks (scintillations events) in the $\frac{d^2\phi_i}{dt^2}$ time series as well as lower noise background and the absence of a low frequency trend. On the other hand, the sampling rate depends on the integration time T_{COR} inside the PLL unit of GPS receiver features. In case of optimal phase discriminator the carrier phase has to be constant during the integration time T_{COR}. In this case, the minimal data sampling rate should be more than $1/T_{COR}$. However, it is not obligatory in the case of a quasi-optimal phase discriminator when the integration time should be within the interval $1ms \leq T_{COR} \leq 20\,ms$. In the last case, the length of a ranging code sequence (1 ms for the CA code) determines the lower limit of the integration time ($T_{COR} = 1$ ms). The final decision about the optimal integration time is limited by two factors: (a) the carrier-to-noise ratio in the phase measuring channel; and (b) the influence of the low-frequency processes on the phase measurement accuracy. The longer integration time yields both the higher carrier-to-noise ratio and the higher phase measurement accuracy. However, with an increase of the accumulation time beyond 10–20 ms, the effects of a reference oscillator instability and Doppler frequency drift can appear. Therefore, the maximal data sampling rate should be 25 Hz or higher to achieve the highest accuracy and sensitivity of the $\frac{d^2\phi_i}{dt^2}$ parameter.

4. The results of efficiency comparison between the $\frac{d^2\phi_i}{dt^2}$ index and another typical ionospheric parameters and scintillation indices (TEC, ROTI, DROTI, *S4*, $\sigma\varphi$) show that "sensitivity" and reliability of each of the indices/parameters differs significantly one from another. In general, it seems that each index has its own "critical" sensitivity of particular ionospheric turbulences depending on the data pre-processing procedures (de-trending and filtering).
5. It was found that the sharp and rapid peaks in the $\frac{d^2\phi_i}{dt^2}$ variations can be related not only to scintillations caused by small-scale ionospheric disturbances but also to multipath and blocked signal effects. It means that local multipath and blocked signal pattern should be tested and excluded before the $\frac{d^2\phi_i}{dt^2}$ data interpreting.

In conclusion, the suggested $\frac{d^2\phi_i}{dt^2}$ index is easy derived from single-frequency carrier phase data. In case of adequate data sampling rate the index provides both reliable detection of the ionospheric scintillation events and the phase time series de-trending with no additional data pre-processing. Thus, the $\frac{d^2\phi_i}{dt^2}$ index is suggested as an independent scintillation indicator and can be considered as an additional tool to be used together with the typical ionospheric scintillation indices.

Acknowlegements

This work was supported by grants 18-35-20038 and 18-05-00343 from Russian Foundation for Basic Research. LANCE acknowledges partial support from CONACyT PN 2015-173, CONACyT-AEM Grant 2017-01-292684, and DGAPA-PAPIIT Grant IN106916. The authors would like to thank the Canadian high arctic ionospheric network (CHAIN) (Jayachandran et al. 2009) for provided 50 Hz GPS data. Other experimental data were obtained from « Angara » Center for Common Use of scientific equipment (http://ckp-rf.ru/ckp/3056/) under budgetary funding of Basic Research program II.12. The OMNI data were obtained from the GSFC/SPDF OMNIWeb interface at http://omniweb.gsfc.nasa.gov.

References

Afanasiev, N. T., Tinin, M. V., & Kolesnik, S. N. (2001). A comparison of results of a numerical simulation and an approximate calculation of statistical characteristics of radio waves in the layer with random inhomogeneities of dielectric permittivity. *Waves in Random Media, 11,* 363–376. https://doi.org/10.1088/0959-7174/11/4/301.

Afraimovich, E. L., Astafyeva, E. I., Demyanov, V. V., & Gamayunov, I. F. (2009). Mid-latitude amplitude scintillation of GPS signals and GPS performance slips. *Advances in Space Research, 43,* 964–972. https://doi.org/10.1016/j.asr.2008.09.015.

Afraimovich, E. L., Demyanov, V. V., & Kondakova, T. N. (2003). Degradation of performance of the navigation GPS system in

geomagnetically disturbed conditions. *GPS Solutions, 7*(2), 109–118. https://doi.org/10.1007/s10291-003-0053-7.

Afraimovich, E. L.. & Perevalova, N. P. (2006). GPS-monitoring of earth upper atmosphere, Irkutsk, Russian Academy of Sciences, Siberian Branch, p. 460. ISBN:5-98277-033-7.

Afraimovich, E. L., et al. (2013). Review of GPS/GLONASS studies of the ionospheric response to natural and anthropogenic processes and phenomena. *Journal of Space Weather and Space Climate, 3,* A27. https://doi.org/10.1051/swsc/2013049.

Benton, C. J., & Mitchell, C. N. (2012). GPS satellite oscillator faults mimicking ionospheric phase scintillation. *GPS Solutions, 16,* 477–482. https://doi.org/10.1007/s10291-011-0247-3.

Benton, C. J., & Mitchell, C. N. (2014). Further observations of GPS satellite oscillator anomalies mimicking ionospheric phase scintillation. *GPS Solutions, 18,* 387–391. https://doi.org/10.1007/s10291-013-0338-4.

Bhattacharrya, A., et al. (2000). Nighttime equatorial ionosphere: GPS scintillations and differential carrier phase fluctuations. *Radio Science, 35*(1), 209–224.

Bougard, B., Sleewaegen, J.M., Spogli, L., Veettil, S.V., Monico, J.F. (2011). CIGALA: Challenging the solar maximum in Brazil with PolaRxS. In: Proceedings of the 24th International Technical Meeting of the Satellite Division of the Institute of Navigation 2011, ION GNSS 2011, pp. 2572–2579.

Briggs, B., & Parkin, I. (1963). On the variation of radio star and satellite scintillations with zenith angle. *Journal of Atmospheric and Terrestrial Physics, 25,* 339–366. https://doi.org/10.1016/00219169(63)90150-8.

De la Luz, V., et al. (2018). First joint observations of space weather events over Mexico. *Annales Geophysicae, 36,* 1347–1360. https://doi.org/10.5194/angeo-36-1347-2018.

Ghoddousi-Fard, R., Prikryl, P., & Lahaye, F. (2013). GPS phase difference variation statistics: A comparison between phase scintillation index and proxy indices. *Advances in Space Research, 52*(8), 1397–1405. https://doi.org/10.1016/j.asr.2013.06.035.

Global Positioning Systems Directorate Systems Engineering and Integration Interface Specification: IS-GPS-200J. 2018.

Gorbunov, M. E., & Gurvich, A. S. (1998). Microlab-1 experiment. Multipath effects in the lower troposphere. *Journal of Geophysical Research: Atmospheres., 103*(12), 3819–13826. https://doi.org/10.1029/98JD00806.

Gulyaeva, T. L., & Stanislawska, I. (2008). Derivation of a planetary ionospheric storm index. *Annal Geophys, 26,* 2645–2648. https://doi.org/10.5194/angeo-26-2645-2008.

Herbster, C. S. (2007). Scintillation effects on national geospatial-intelligence agency (NGA) GPS monitor stations. Proc. of the Int. Beacon Satellite Symp., by Doherty P.H. (ed), Boston College, Boston.

Hofmann-Wellenhof, B., Lichtenegger, H., & Wasle, E. (2008). *GNSS Global navigation satellite systems; GPS, Glonass, Galileo & more*. New York: Springer. https://doi.org/10.1007/978-3-211-73017-1.

Jacobsen, K. S. (2014). The impact of different sampling rates and calculation time intervals on ROTI values. *Journal of Space Weather and Space Climate, 4*(2014), A33. https://doi.org/10.1051/swsc/2014031.

Jakowski, N., Borries, C., & Wilken, V. (2012). Introducing a disturbance ionosphere index (DIX). *Radio Science, 47,* RS0L14. https://doi.org/10.1029/2011rs004939.

Jayachandran, P. T., Langley, R. B., MacDougall, J. W., Mushini, S. C., Pokhotelov, D., Hamza, A. M., et al. (2009). The Canadian high arctic ionospheric network (CHAIN). *Radio Science, 44,* RS0A03. https://doi.org/10.1029/2008RS004046.

Jin, S. G., Jin, R., & Li, D. (2017). GPS detection of ionospheric Rayleigh wave and its source following the 2012 Haida Gwaii earthquake. *Journal of Geophysical Research: Space Physics, 122*(1), 1360–1372. https://doi.org/10.1002/2016ja023727.

Jorgenson, P. S. (1978). Ionosphere measurements from NAVSTAR satellites: SAMSO-TR-29, AD A068809. V. A. P. 22304.

Juan, J. M., Sanz, J., Rovira-Garcia, A., González-Casado, G., Ibáñez, D., & Perez, R. O. (2018a). AATR an ionospheric activity indicator specifically based on GNSS measurements. *J Space Weather Space Climate, 8,* A14. https://doi.org/10.1051/swsc/2017044.

Juan, J. M., et al. (2018b). Feasibility of precise navigation in high and low latitude regions under scintillation conditions. *Journal of Space Weather and Space Climate, 8,* A05. https://doi.org/10.1051/swsc/2017047.

Kaplan, E. D. (1996). Understanding GPS: Principles and Applications. Artech House, pp. 556.

Kintner, P. M., Kil, H., & de Paula, E. (2001). Fading time scales associated with GPS signals and potential consequences. *Radio Science, 36*(4), 731–743.

Kolesnik, S. N., Tinin, M. V., & Afanasiev, N. T. (2002). Statistical characteristics of a wave propagating through a layer with random irregularities. *Waves in Random Media, 12,* 417–431. https://doi.org/10.1088/0959-7174/12/4/302.

Ledvina BM, Makela JJ, and Kintner PM (2002) First observations of intense GPS L1 amplitude scintillations at multitude. Geophysical. Res. Lett. 29 (14). https://doi.org/10.1029/2002GL014770.

Matsumura, M., et al. (2011). Numerical simulations of atmospheric waves excited by the 2011 off the Pacific coast of Tohoku Earthquake. *Earth Planets Space, 63,* 885–889.

McCaffrey, A. M., & Jayachandran, P. T. (2017). Spectral characteristics of auroral region scintillation using 100 Hz sampling. *GPS Solutions, 21,* 1883–1894. https://doi.org/10.1007/s10291-017-0664-z.

McCaffrey, A. M., Jayachandran, P. T., Langley, R. B., & Sleewaegen, J. M. (2018). On the accuracy of the GPS L2 observable for ionospheric monitoring. *GPS Solutions, 22,* 23. https://doi.org/10.1007/s10291-017-0688-4.

Mendillo, M., Lin, B., & Aarons, J. (2000). The application of GPS observations to equatorial aeronomy. *Radio Science, 35*(3), 885–904. https://doi.org/10.1029/1999RS002208.

OMNI-web data base. https://omniweb.gsfc.nasa.gov/form/dx1.html. Accessed 29 Jan 2018.

Pavelyev, A. G., Liou, Y. A., Wickert, J., Schmidt, T., & Pavelyev, A. A. (2010). Phase acceleration: a new important parameter in GPS occultation technology. *GPS Solutions, 14,* 3–11. https://doi.org/10.1007/s10291-009-0128-1.

Pi, X., Mannucci, A. J., Lindqwister, U. J., & Ho, C. M. (1997). Monitoring of global ionospheric irregularities using the worldwide GPS-network. *Geophysical Research Letter, 24,* 2283–2286. https://doi.org/10.1029/97GL02273.

Piersanti, M., Alberti, T., Bemporad, A., Berrilli, F., Bruno, R., Vincenzo, C., et al. (2017). Comprehensive analysis of the geoeffective solar event of 21 June 2015: Effects on the magnetosphere, plasmasphere, and ionosphere systems. *Solar*

Physics, 292(11), 169. https://doi.org/10.1007/s11207-017-1186-0.

Prikryl, P., Ghoddousi-Fard, R., Weygand, J. M., Viljanen, A., Connors, M., Danskin, D. W., et al. (2016). GPS phase scintillation at high latitudes during the geomagnetic storm of 17–18 March 2015. *Journal of Geophysical Research: Space Physics, 121*(10), 448–465. https://doi.org/10.1002/2016JA023171.

Priyadarshi, S., Zhang, Q. H., Thomas, E. G., Spogli, L., & Cesaroni, C. (2018). Polar traveling ionospheric disturbances inferred with the B-spline method and associated scintillations in the Southern Hemisphere. *Advances in Space Research, 62*(11), 3249–3266. https://doi.org/10.1016/j.asr.2018.08.015.

Tiwari, R., & Strangeways, H. J. (2015). Regionally based alarm index to mitigate ionospheric scintillation effects for GNSS receivers. *Space Weather, 13,* 72–85. https://doi.org/10.1002/2014SW001115.

Tsugawa, T., Saito, A., Otsuka, Y., Nishioka, M., Maruyama, T., Kato, H., et al. (2011). Ionospheric disturbances detected by GPS total electron content observation after the 2011 off the Pacific coast of Tohoku Earthquake. *Earth Planets Space, 63,* 875–879.

Van Dierendonck, A. J., Klobuchar, J., Hua, Q. (1993). Ionospheric scintillation monitoring using commercial single frequency C/A code receivers. In: Proceedings of ION GPS 1993, Salt Lake City, Utah, pp 1333–1342. https://www.semanticscholar.org/paper/Ionospheric-Scintillation-Monitoring-Using-Single-C-Van-John/9ddb800085b45cfea5a579f45c095d99a9df315b.

Voeykov, S. V., Yasyukevich, A. S., Edemskiy, I. K., Perevalova, N. P., & Yasyukevich, Y. U. V. (2018). WTEC: A new index to estimate the intensity of ionospheric disturbances. *Results in Physics, 11,* 1056–1057. https://doi.org/10.1016/j.rinp.2018.11.023.

Wilken, V., Kriegel, M., Jakowski, N., & Berdermann, J. (2018). An ionospheric index suitable for estimating the degree of ionospheric perturbations. *Journal of Space Weather and Space Climate, 8,* A19. https://doi.org/10.1051/swsc/2018008.

Cai, C., Liu, Z., Pengfei, X., & Wujiao, D. (2013). Cycle slip detection and repair for undifferenced GPS observations under high ionospheric activity. *GPS Solutions, 17,* 247–260. https://doi.org/10.1007/s10291-012-0275-7.

PolaRxS SBF Reference Guide for version 2.9.0 of the GNSS Firmware. from http://chain.physics.unb.ca/docs/septentrio/PolaRxS-Firmware-v2.9.0-SBF-Reference-Guide.pdf.

Yasyukevich, Y. U. V. (2017). The 50 Hz JAVAD Data Set for the case study. https://doi.org/10.5281/zenodo.848325. Accessed 30 Aug 2017.

Yasyukevich, Yu V, Vesnin, A. M., & Perevalova, N. P. (2018). SibNet—Siberian global navigation satellite system network: Current state. *Solar-Terrestrial Physics, 4*(4), 63–72. https://doi.org/10.12737/stp-44201809.

Yeh, C. K., Liu, C. H. (1982). Radio wave scintillations in the ionosphere. In: Proc. IEEE 70(4):324-360. https://doi.org/10.1109/PROC.1982.1231.

(Received February 10, 2019, revised July 2, 2019, accepted July 10, 2019, Published online July 29, 2019)